Int. J. Electrochem. Sci., 15 **(2020)** 5208 – 5219, doi: 10.20964/2020.06.37

International Journal of
ELECTROCHEMICAL
SCIENCE
www.electrochemsci.org

The Inhibition Effect of 2-amino-4-chlorobenzothiazole on X65 Steel Corrosion in H_2SO_4 Solution

Shujun Chen[1,*], *Siyi Chen*[1], *Huajun Zhao*[1], *Hao Wang*[1], *Pushan Wen*[1], *Hao Li*[2]

[1] School of Chemistry and Chemical Engineering, Zunyi Normal University, Zunyi 563006, China
[2] School of Chemistry and Chemical Engineering, Chongqing University, Chongqing 400044, China
[*]E-mail: shujunchen_znu@163.com

Received: 15 January 2020 / *Accepted:* 12 March 2020 / *Published:* 10 May 2020

In this study, we study 2-amino-4-chlorobenzothiazole (ACBT) as a corrosion inhibitor for X65 steel in H_2SO_4 medium. The corrosion inhibition performance of ACBT for X65 steel has been studied using electrochemical methods, surface morphology analysis and theoretical calculations. Electrochemical experiment data indicated ACBT belongs to mixed-type corrosion inhibitor. When the concentration of ACBT is 5 mM at 298 K, its corrosion inhibition efficiency is close to 90%. The potentiodynamic polarization curve shows that the inhibition effect of ACBT on the cathodic reaction is significantly greater than that of the anodic reaction. SEM morphology analysis strongly proves the corrosion inhibition performance of ACBT. Quantum chemical calculations and molecular dynamics simulations have revealed the corrosion inhibition properties of ACBT. The adsorption of ACBT on the surface of X65 steel conforms to the Langmuir adsorption isothermal model.

Keywords: Corrosion inhibitor; X65 steel; potentiodynamic polarization curve; Quantum chemical calculations; Langmuir adsorption.

1. INTRODUCTION

The X65 steel is widely used in natural gas and oil pipelines, construction, military, marine and many other fields [1]. This is due to its good corrosion resistance performance and its low price. However, X65 steel is still susceptible to corrosion in a complex and variable working environment. Corroded X65 steel poses a potential threat to the working environment and can cause significant economic losses [2]. Therefore, in order to effectively inhibit the corrosion of X65 steel, corrosion scientists have developed and explored many corrosion protection methods. Common corrosion protection methods include coatings, corrosion inhibitors, sacrificial anodes, etc. Among them, the corrosion inhibitor has a small amount, has a significant effect, and is inexpensive [3]. Therefore, corrosion inhibitors have become one of the most important corrosion protection methods.

The corrosion inhibitors are divided into organic corrosion inhibitors and inorganic corrosion inhibitors. Due to the large amount of inorganic corrosion inhibitor, it can have a great impact on the environment, so its application is greatly restricted [4]. In contrast, organic corrosion inhibitors, due to their small amounts, have a small impact on the environment and are easier to meet the needs of industry. Organic corrosion inhibitors usually contain heteroatoms such as nitrogen, oxygen, sulfur and polar functional groups [5-9]. These polar functional groups and heteroatoms contain lone electron pairs, which can form coordination bonds with 3d empty orbitals in iron atoms. Thus, a dense and ordered molecular barrier film is formed on the surface of X65 steel, thereby effectively inhibiting the corrosion of X65 steel.

In this paper, the corrosion inhibition performance of ACBT on X65 steel in sulfuric acid solution was studied by various experimental methods. The molecules of ACBT are shown in Figure 1, purchased from Adamas Reagent Company. We can clearly find that the ACBT molecule contains one sulfur atom and two nitrogen atoms, so it has potential as a corrosion inhibitor. The experimental methods include electrochemical methods, surface morphology analysis, and quantum chemical calculations and molecular dynamics simulations. That is to say, we have thoroughly explored the corrosion inhibition performance of ACBT on X65 steel from both experimental and theoretical aspects.

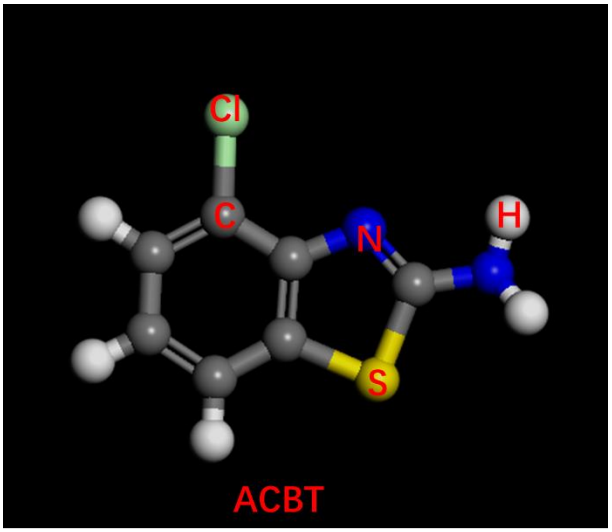

Figure 1. Molecular chemical structure of 2-amino-4-chlorobenzothiazole (ACBT)

2. EXPERIMENTAL

2.1. Materials and regents

The used compound ACBT was used directly without further purification. The 0.5 M H_2SO_4 solution was treated as corrosive solution or the blank solution. The deionized water was used as solvent. The test solution was 0.5 M H_2SO_4 solution with different concentrations (0.25 mM, 0.5 mM, 1 mM, 2

mM, 5 mM) of ACBT. The water bath can control the experimental temperature. Besides, X65 steel was the selected metal material.

2.2. Electrochemical methods

For electrochemical tests, 400, 1200, 2000, and 3000 grades of emery papers were used to remove the oxide layer on X65 steel surface. Then the specimens were rinsed with deionized water and ethanol, and finally dried. The samples were dried for using in next. A three-electrode system was applied to do electrochemical tests by CHI 660E electrochemical station at 298 K. X65 steel, saturated calomel electrode (SCE), and Pt sheet were utilized as the working electrode, reference electrode, and the counter electrode, respectively. EIS was recorded at an open circuit potential (OCP) within a frequency range of 100 kHz to 0.01 Hz with 5 mV peak-to-zero perturbation. Polarization was measured at the sweep rate of 1.0 mV/s at the range of ±250 mV of OCP. The inhibition efficiencies from different methods are calculated by [10-20],

$$\eta_{\mathrm{EIS}}(\%) = (1 - \frac{R_{ct,0}}{R_{ct}}) \times 100 \quad (1)$$

$$\eta_{\mathrm{Tafel}}(\%) = (1 - \frac{i_{corr}}{i_{corr,0}}) \times 100 \quad (2)$$

where $R_{ct,0}$ and R_{ct} are charge transfer resistances of X65 steel in blank solution and inhibitor containing solution, $i_{corr,0}$ and i_{corr} show current densities of X65 steel in blank solution and inhibitor containing solution, respectively.

2.3. SEM method

Scanning electron microscope (SEM) surface topography was carried out by immersing X65 steel sample in the test solution in the absence and presence of 5 mM ACBT at 298 K for 8 h. The instrument model used for SEM studies is JEOL-JSM-7800F.

2.4. Calculation methods

Density functional theory (DFT) is a popular technique to predict the chemical activity of inhibitor molecules. In this study, dmol3 on DNP/BLYP was used to optimize the molecular structure of neutral and protonated ACBT. The optimized frontier molecular orbital were obtained. The quantum chemical parameters including the energy of highest occupied molecular orbital (E_{HOMO}), the energy of lowest unoccupied molecular orbital (E_{LUMO}), energy gap (ΔE) , and the dipole moment (μ) were obtained. Molecular dynamics simulations were carried out in a simulation box with periodic boundary conditions using Forcite to explore the interaction between ACBT and Fe (110) surface. NVT canonical ensemble and COMPASS force field were used. The final adsorption configuration and interaction energy were obtained.

3. RESULTS AND DISCUSSION

3.1. EIS measurement

Figure 2 shows Nyquist plots of ACBT on X65 steel in 0.5M sulfuric acid solution at 298K. We can find that as the ACBT concentration increases, the radius of the capacitive loops arc increases significantly. The increase of the capacitive loops arc radius indicates that the charge transfer resistance on the surface of X65 steel increases, which increases the corrosion resistance of X65 steel in sulfuric acid solution. In addition, it is worth mentioning that all capacitive loops arcs show an imperfect semicircle, which indicates that the adsorption of ACBT on the surface of X65 steel makes the surface uneven. In addition, the shape of all capacitive arcs did not change significantly, which indicates that the adsorption mechanism of ACBT on the surface of X65 steel did not change its reaction mechanism[21].

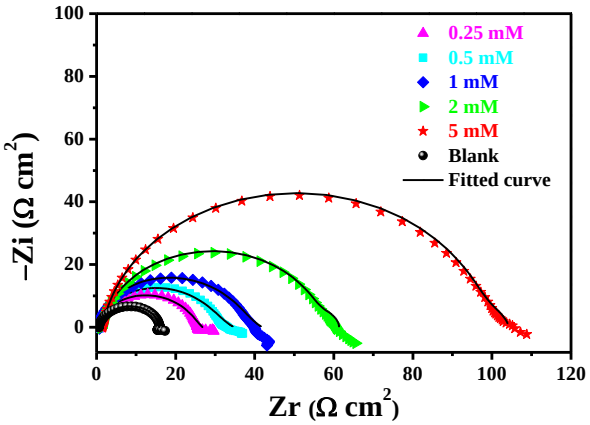

Figure 2. The Nyquist plots for X65 steel with different concentrations of ACBT in 0.5 M H_2SO_4 solution

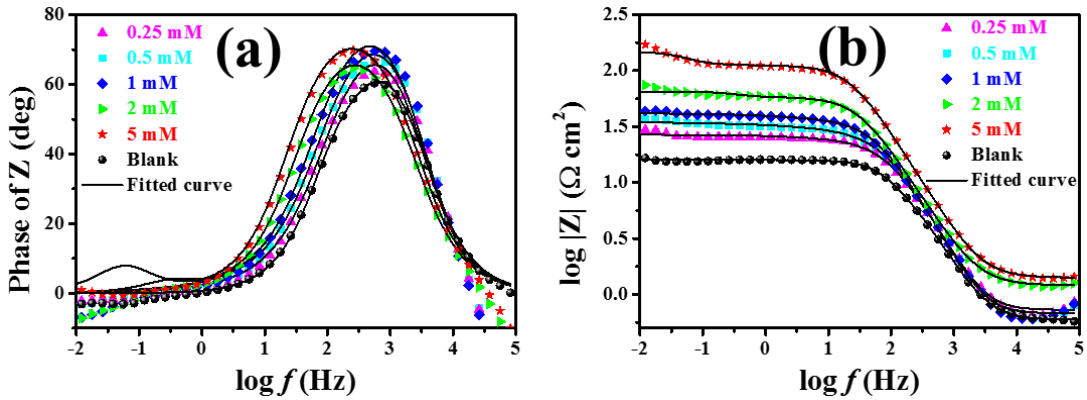

Figure 3. Bode plots for X65 steel electrode with different concentrations of ACBT in 0.5 M H_2SO_4 solution

Figure 3 (a) and (b) shows the phase angle diagram and impedance mode diagram of ACBT in sulfuric acid solution, respectively. As shown in Figure 3 (a), as the ACBT concentration increases, the

phase angle diagram becomes higher and wider, which indicates that the adsorption of ACBT on X65 steel increases the corrosion resistance of X65 steel. Figure 3 (b) shows the impedance modulus of AC65 versus X65 steel in sulfuric acid solution. It can be found that in the low frequency region, the impedance mode value increases by an order of magnitude. This shows that ACBT shows excellent corrosion inhibition performance for X65 steel in sulfuric acid solution.

In order to quantitatively analyze the corrosion inhibition performance of ACBT on X65 steel in sulfuric acid solution, we used the equivalent circuit diagram in Figure 4 for quantitative analysis. Among them, R_{ct} is a charge transfer resistance, which can measure the corrosion resistance of X65 steel. R_s is the solution resistance, which represents the solution resistance from the reference electrode to the X65 working electrode. R_f is the film resistance of X65 steel surface. The fitted electrochemistry parameters are listed in Table 1. The fitted chi-square value is less than 10^{-2}, which indicates that the error between the experimental value and the fitted value is small. It can be found that the charge transfer resistance in the blank solution is 11.58 Ω cm^2 in the Table 1. When the ACBT concentration is 5 mM, the value of the charge transfer resistance sharply increases to 110.9 Ω cm^2. The corrosion inhibition efficiency at this time is 89.6%.

In Table 1, the C_{dl} can be gained according to the this formula [22, 23]:

$$C = Y_0(\omega)^{n-1} = Y_0(2\pi f_{Z_{im-Max}})^{n-1} \quad (3)$$

where ω stands for angular frequency. n is phase transfer ($-1 \le n \le 1$).

From Table 1, it can be found that the C_{dl} values in the blank solution is 145.7 μF cm^{-2}. As the concentration of ACBT increases, the C_{dl} values show a downward trend. When the DDA concentration is 5 mM, the value of C_{dl} drops sharply to 23.3 μF cm^{-2}. This experiment data can be explained using the Helmholtz model [24]:

$$C_{dl} = \frac{\varepsilon^0 \varepsilon}{d} S \quad (4)$$

where ε and ε^0 stand for the local and air dielectric constant of the electric double layer, respectively, S is the X65 steel electrode surface area, and d is the thickness of the electric double layer. The value of ε of ACBT is smaller than that of H_2O, and the volume is obviously larger than that of H_2O. Therefore, after ACBT replaces the water molecules on the surface of X65 steel, the ε^0 becomes smaller and the thickness of the electric double layer capacitor increases. The more water molecules ACBT replaces the surface of X65 steel, the more obvious the value of C_{dl} decreases.

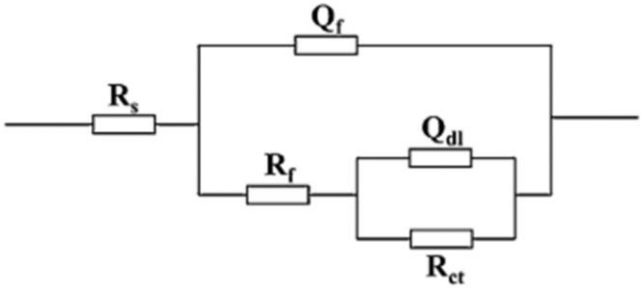

Figure 4. The used electrical circuit to fit EIS.

Table 1. AC Impedance parameters of X65 steel in acid with different concentration of ACBT in 0.5 M H_2SO_4 solution

C (mM)	R_s (Ω cm^2)	R_f (Ω cm^2)	R_{ct} (Ω cm^2)	$Y_0\times10^{-6}$ (Ω^{-1} cm^{-2} s$^{\alpha}$)	n	C_{dl} (μF cm^{-2})	η (%)
Blank	0.60	3.71	11.58	145.7	0.94	278.0	–
0.25	0.69	0.50	26.15	108.2	0.50	67.8	55.7
0.5	0.62	1	34.11	101.2	0.41	69.8	66.1
1	0.61	0.66	41.28	85.6	0.41	72.1	71.9
2	1.2	6.76	57.38	46.6	0.90	49.9	79.8
5	1.4	34.85	110.90	23.3	0.92	19.5	89.6

3.2. Potentiodynamic polarization

Figure 5 shows the potentiodynamic polarization curve of ACBT on X65 steel in sulfuric acid solution. As shown in Figure 5, as the ACBT concentration increases, it can be found that the corrosion current density increases significantly. In addition, it is worth mentioning that the polarization curve of the cathodic branch decreases significantly more than the anodic branch. This shows that after ACBT adsorb on the surface of X65 steel, the inhibition of cathodic hydrogen evolution on the X65 steel is significantly greater than the precipitation of anodic iron ions. The cathodic polarization curves all show a parallel trend, which indicates that ACBT is geometrically cover on the surface of X65 steel.

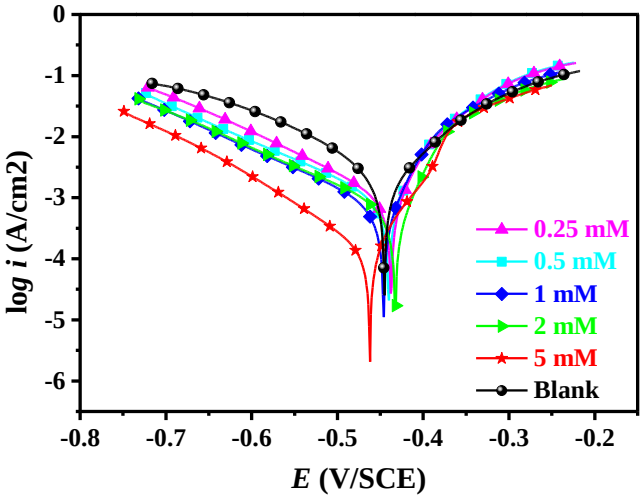

Figure 5. Polarization curves of X65 steel with different concentration of ACBT in 0.5 M H_2SO_4 solution.

In addition, we have used Tafel extrapolation to obtain the corresponding electrochemical parameters, which include corrosion current density, corrosion potential, anodic slope and cathodic slope. In the blank solution without ACBT added, the value of the corrosion potential was –0.445 V, and

the corrosion potential gradually decreased as the concentration of ACBT increased. While the magnitude of the change is significantly less than 85 mV. it indicates that ACBT is a mixed type of corrosion inhibitor for X65 steel in sulfuric acid medium [25]. In addition, it is worth mentioning that when the concentration of ACBT is 5 mM, the corrosion inhibition efficiency is as high as 93.9%. This shows that ACBT can show excellent corrosion inhibition performance for X65 steel in H_2SO_4 medium.

Table 2. Polarization parameters for X65 steel in H_2SO_4 solution without and with ACBT in 0.5 M H_2SO_4 solution at 298 K.

C (mM)	E_{corr}(V/SCE)	i_{corr}(μA cm^{-2})	β_c(mV dec^{-1})	β_a(mV dec^{-1})	η (%)
Blank	−0.445	2468	−140	99	—
0.25	−0.438	1480	−145	93	40.0
0.5	-0.440	1097	−161	65	55.6
1	-0.446	916.4	−159	84	62.9
2	−0.433	549.4	−166	49	77.7
5	-0.462	151.3	−112	48	93.9

3.3. Langmuir study

In order to further study the mechanism of adsorption ACBT in X65 steel surface, we used numerous adsorption isotherm models to explore the adsorption mechanism. We used EIS experimental data to study the isothermal adsorption model. The fitting results show that the ACBT adsorption on the X65 steel surface conforms to the Langmuir adsorption model. The Langmuir adsorption isotherm and ΔG_{ads}^0 expressions are shown below [26-29]:

$$\frac{\theta}{1-\theta} = K_{ads}C \quad (5)$$

$$K_{ads} = \frac{1}{55.5}\exp(-\frac{\Delta G_{ads}^0}{RT}) \quad (6)$$

where C stands for the concentration of ACBT. K_{ads} stands for the adsorption equilibrium constant. θ is the coverage. We used the impedance spectrum experimental data to fit. The fitted linear regression coefficient (R^2) is 0.99933. This indicates that the fit error is small. The fitted results are listed in Figure 6. The value of K_{ads} is 3.87×10^3 L/mol, and it is generally believed that a large K_{ads} value indicates that ACBT can produce a close adsorption on theX65 steel surface. In addition, the ΔG_{ads}^0 value is –30.42 kJ/mol. Negative ΔG_{ads}^0 value manifests that the adsorption of ACBT on the surface of Q235 steel is autonomous. Besides, when the ΔG_{ads}^0 value is greater than –20 kJ/mol, it manifests that the adsorption of corrosion inhibitor on the surface of metal belongs to physical adsorption. When the value of $\Delta G_{ads}^0 \leq$ –40 kJ/mol, the adsorption of corrosion inhibitor on the metal surface is chemical adsorption. When the value of –20 kJ/mol $\leq \Delta G_{ads}^0 \leq$ –40 kJ/mol, the adsorption of corrosion inhibitor on the surface of metal belongs to the interaction of physicochemical adsorption [30-32]. Therefore, the ACBT adsorption on the surface of X65 steel belongs to the interaction of physicochemical adsorption.

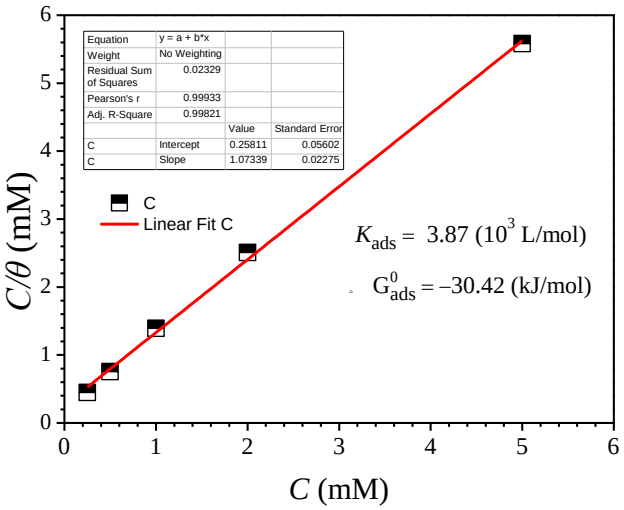

Figure 6. Langmuir adsorption isotherm for X65 steel in 0.5 M H_2SO_4 solution with different concentrations of ACBT.

3.4. DFT calculation

Quantum chemical calculation is an effective way to predict the corrosion inhibition of corrosion inhibitor molecules. It can effectively predict the corrosion inhibition performance of the corrosion inhibitor by the nature of the corrosion inhibitor molecule, thereby saving a lot of material and financial resources. In this work, we calculated the frontier molecular orbitals, dipole moments, and electrostatic potential maps of ACBT molecule. The result of the calculation is presented in Figure 7.

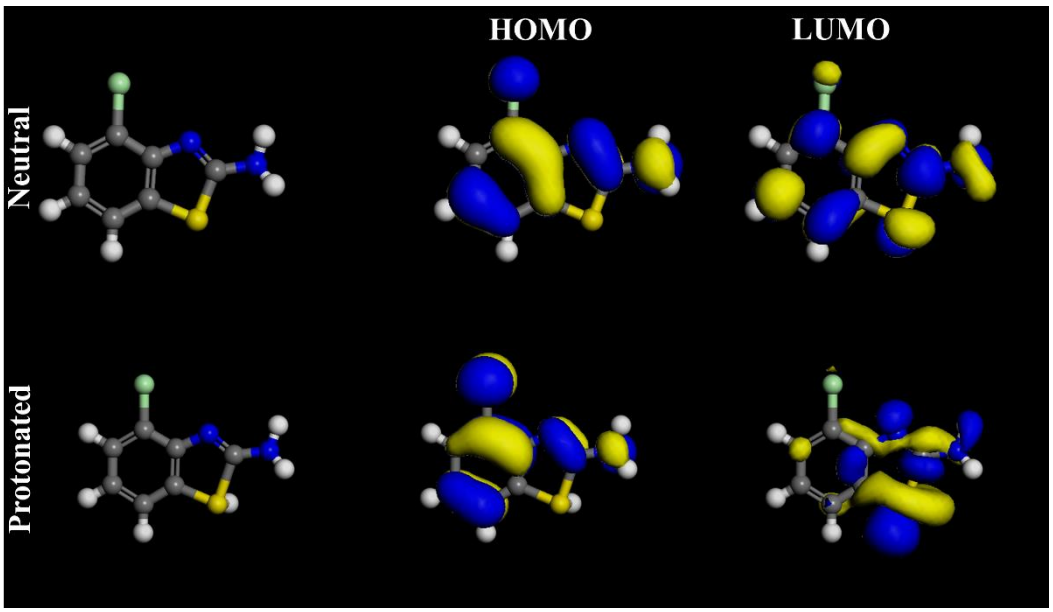

Figure 7. The molecular frontier orbital diagrams of ACBT and $ACBTH^+$ based on DFT theory.

Frontier molecular orbital theory is widely used to study the electron cloud density distribution of corrosion inhibitor molecules. The electron cloud density of ACBT molecule distributed on the whole molecule. This shows that ACBT can be adsorbed on the surface of X65 steel in parallel. The energy gap values ($\Delta E = E_{LUMO} - E_{HOMO}$) of ACBT and $ACBTH^+$ are 2.94 and 2.72 eV in the Table 3. According to the references, usually a small gap value indicates that the corrosion inhibitor molecule has high corrosion inhibition performance [33-35]. Therefore, ACBT being protonated can show better corrosion inhibition performance.

The dipole moment of ACBT and $ACBTH^+$ are 3.04 and 18.07 Debye in the Table 3. Most corrosion workers believe large dipole moments correspond to superior anti-corrosion performance [36, 37]. We can find that dipole moment value of ACBT increases sharply after protonation, which strongly proves that $ACBTH^+$ can show excellent corrosion inhibition performance.

Table 3. The DFT quantum chemical parameters of ACBT and $ACBTH^+$.

E_{HOMO}(eV)	E_{LUMO}(eV)	ΔE(eV)	μ(D)
–4.46	–1.52	2.94	3.04
–9.85	–7.13	2.72	18.07

3.5. Molecular dynamics simulation

We used molecular dynamics simulation (MDS) to calculate the adsorption of ACBT on Fe (110) surface. Figure 8 presents the ACBT and $ACBTH^+$ molecules on the ideal surface of Fe (110) under air environment and solution conditions, respectively.

It can be found that ACBT and $ACBTH^+$ are adsorbed on the Fe (110) surface in parallel under both vacuum and solution conditions. This adsorption model can obtain maximum coverage to protect X65 steel. This is consistent with the results predicted by quantum chemistry calculations and molecular dynamics models.

The adsorption energy of ACBT on surface of Fe (110) can be obtained by the following formulas [38, 39]:

$$E_{\text{int}\,eract} = E_{tot} - (E_{subs} + E_{inh}) \quad (7)$$

$$E_{binding} = -E_{\text{int}\,eract} \quad (8)$$

Here, $E_{binding}$ stands for the binding energy of ACBT and Fe (110), E_{tot} stands for the total energy, E_{subs} is the energy of the Fe (110) or all H_2O molecules, E_{inh} is the ACBT energy. The binding energy values of ACBTH and $ACBTH^+$ on the surface of Fe (110) are 345.4 kJ/mol and 378.9 kJ/mol in vacuum environment. The binding energy values of ACBT and $ACBTH^+$ on the surface of Fe (110) are 425.5 kJ/mol and 470.2 kJ/mol in solution environment. This reveals that the ACBT has a forceful adsorption ability on the surface of Fe (110), thus exhibiting distinguished corrosion inhibition performance [40, 41].

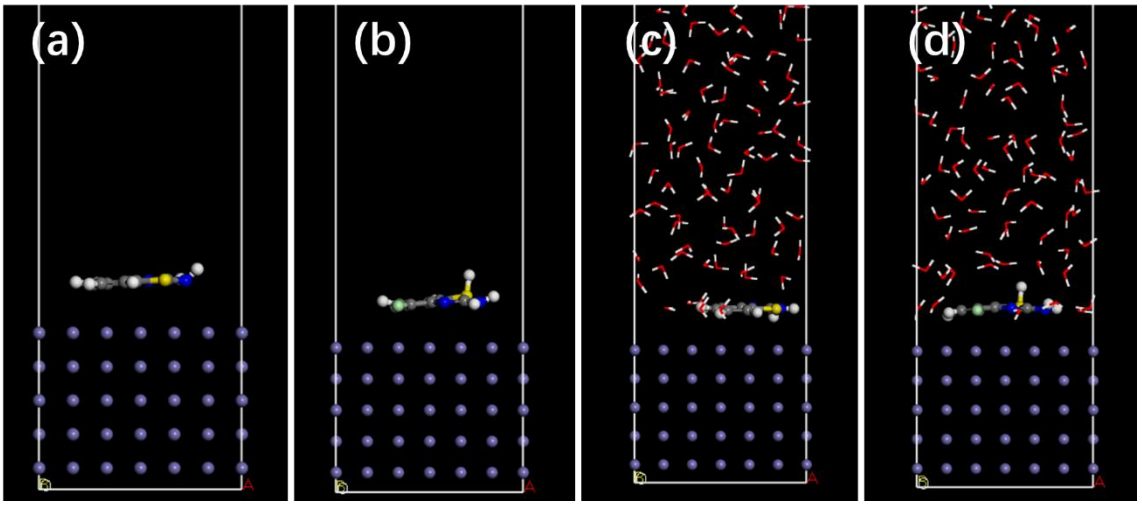

Figure 8. The final snapshots of neutral and protonated ACBT over Fe (110) surface obtained from MD simulations, (a) neutral ACBT, without water molecules, (b) protonated ACBT, with water molecules, (c) neutral ACBT, without water molecules, (d) protonated ACBT, with water molecules.

3.6. SEM observation

Figure 9 is topography maps the X65 steel samples immersed in 0.5 mol/L sulfuric acid solution with and without 5 mM for 8 hours at 298 K. Figure 9 (a) is the surface topography of X65 steel immersed in the blank solution. It can be found that there are obvious corrosion holes on the surface of X65 steel. Figure 9 (b) is the topography map of X65 steel immersed in 0.5 M H_2SO_4 with 5 mM ACBT at 298 K. It can be found that there are no obvious corrosion holes on the entire surface. This strongly proves that ACBT can effectually restrain the steel corrosion in acid media after adsorption on the X65 steel surface.

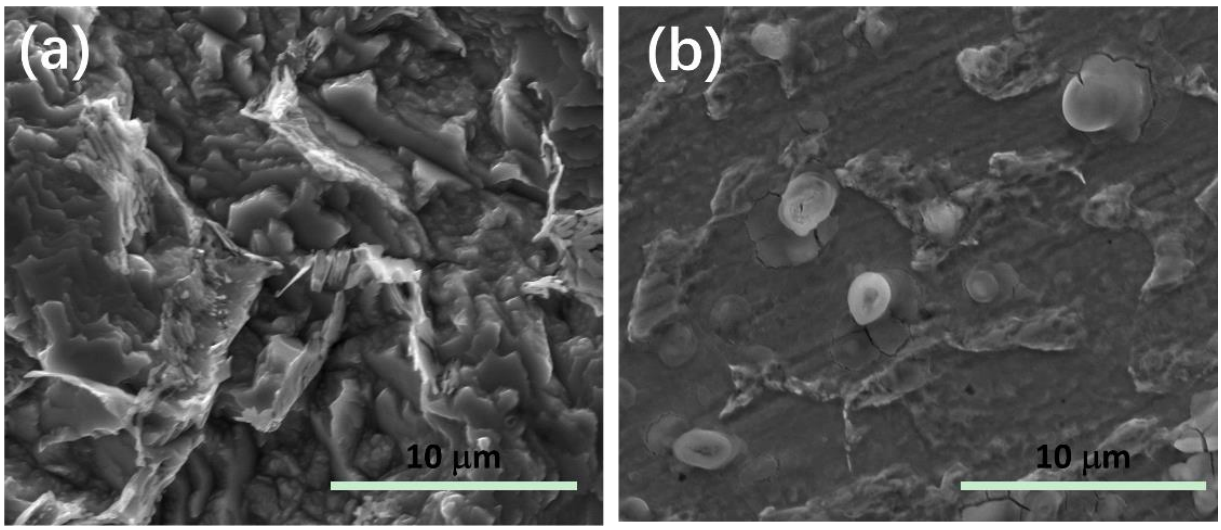

Figure 9. SEM images of X65 steel without (a) and with (b) addition of ACBT in 0.5 M H_2SO_4 solution

4. CONCLUSIONS

ACBT exhibits excellent anti-corrosion nature of X65 in 0.5 mol/L H_2SO_4. Electrochemical experiments data show that ACBT can restrain the cathodic and anodic reaction of X65 steel, which is a mixed-type corrosion inhibitor. SEM morphology analysis strongly and vividly support the results of electrochemical tests. The adsorption of ACBT on the X65 steel surface is consistent with Langmuir adsorption. Its adsorption type is a combination of physicochemical adsorption. Quantum chemical calculations strongly explore the active adsorption sites of ACBT molecule. Molecular dynamics simulations show that ACBT adsorbs on the Fe (110) surface in parallel model to obtain the largest coverage area.

ACKNOWLEDGEMENTS
The authors gratefully appreciate the financial support provided the Natural Science Research Project of Guizhou Department of Education (Qian jiaohe KY [2019]123), Natural Science Research Project of Zunyi Normal University (Zunyi Normal University BS[2019]11), and United Science Research Project of Zunyi Science and Technology and Zunyi Normal University (Zunshi Kehe HZ 270), National Science Foundation of China (21766040) and Natural Science Research Project of Guizhou Education Department ([2019]058).

References

1. B. Tan, S. Zhang, H. Liu, Y. Guo, Y. Qiang, W. Li, L. Guo, C. Xu, and S. Chen, *J. Colloid. Interf. Sci.,* 538 (2019) 519.
2. K. Shalabi, A.M. Helmy, A.H. El-Askalany, and M.M. Shahba, *J. Mol. Liq.,* 293 (2019) 111480.
3. M.n. Corrales-Luna, M.T. Le, and E.M. Arce-Estrada, *Int. J. Electrochem. Sci.,* 14 (2019) 4420.
4. Y. Qiang, S. Zhang, L. Wang, *Appl. Surf. Sci.,* 492 (2019) 228.
5. B. Tan, S. Zhang, Y. Qiang, L. Feng, C. Liao, Y. Xu, and S. Chen, *J. Mol. Liq.,* 248 (2017) 902.
6. Y. Qiang, S. Zhang, H. Zhao, B. Tan, L. Wang, *Corros. Sci.,* 161 (2019) 108193.
7. E. A. Flores-Frias, V. Barba , M.A. Lucio-Garcia, R. Lopez-Cecenes, J. Porcayo-Calderon, and J.G. Gonzalez-Rodriguez, *Int. J. Electrochem. Sci.,* 14 (2019) 5026.
8. S. Y. Al-Nami, *Int. J. Electrochem. Sci.,* 14 (2019) 3986.
9. Ž.Z. Tasić, M.B. Petrović Mihajlović, M.B. Radovanović, A.T. Simonović, and M.M. Antonijević, *J. Mol. Struct.,* 1159 (2018) 46.
10. B. Tan, S. Zhang, Y. Qiang, L. Guo, L. Feng, C. Liao, Y. Xu, and S. Chen, *J. Colloid Interf. Sci.,* 526 (2018) 268.
11. Y. Qiang, S. Zhang, B. Tan, and S. Chen, *Corros. Sci.,* 133 (2018) 6.
12. Y. Qiang, S. Fu, S. Zhang, S. Chen, and X. Zou, *Corros. Sci.,* 140 (2018) 111.
13. J. Du, Y. Liu, P. Liu, Y. Liu, S. Gao, and L. Zhang, *Int. J. Electrochem. Sci.,* 14 (2019) 4532.
14. F. H. Al-abdali, M. Abdallah, and R. El-Sayed, *Int. J. Electrochem. Sci.,* 14 (2019) 3509.
15. Ž.Z. Tasić, M.B. Petrović Mihajlović, M.B. Radovanović, and M.M. Antonijević, *J. Mol. Liq.,* 265 (2018) 687.
16. M.B. Petrović Mihajlović, M.B. Radovanović, Ž.Z. Tasić, and M.M. Antonijević, *J. Mol. Liq.,* 225 (2017) 127.
17. M.B. Radovanović, and M.M. Antonijević, *J. Adhes. Sci. Technol.,* 31 (2016) 369.
18. M.T. Zaky, M.I. Nessim, and M.A. Deyab, *J. Mol. Liq.,* 290 (2019) 111230.
19. G. Vengatesh, and M. Sundaravadivelu, *J. Mol. Liq.,* 287 (2019).

20. Z. Sanaei, G. Bahlakeh, B. Ramezanzadeh, and M. Ramezanzadeh, *J. Mol. Liq.*, 290 (2019) 111176.
21. S. Xu, W. Li, X. Zuo, D. Zheng, X. Zheng, and S. Zhang, *Int. J. Electrochem. Sci.*, 14 (2019) 5777.
22. B. Tan, S. Zhang, W. Li, X. Zuo, Y. Qiang, L. Xu, J. Hao, S. Chen, *J. Ind. Eng. Chem.*, 77 (2019) 449.
23. M. Talari, S. Mozafari Nezhad, S.J. Alavi, M. Mohtashamipour, A. Davoodi,and S. Hosseinpour, *J. Mol. Liq.*, 286 (2019) 110915.
24. B. Tan, S. Zhang, H. Liu, Y. Qiang, W. Li, L. Guo, and S. Chen, *J. Taiwan Inst. Chem. E.*, 102 (2019) 424.
25. Y. Qiang, S. Zhang, L. Guo, X. Zheng, B. Xiang, and S. Chen, *Corros. Sci.*, 119 (2017) 68.
26. Y. Qiang, S. Zhang, L. Guo, S. Xu, L. Feng, I.B. Obot, and S. Chen, *J. Clean. Prod.*, 152 (2017) 17.
27. H. M. Elabbasy, and A.S. Fouda, *Int. J. Electrochem. Sci.*,14 (2019) 3684.
28. Z.Z. Tasic, M.M. Antonijevic, M.B. Petrovic Mihajlovic, and M.B. Radovanovic, *J. Mol. Liq.,* 219 (2016) 463.
29. L. Gao, S. Peng, X. Huang, and Z. Gong, *Appl. Surf. Sci.*, 511 (2020).
30. X. Zhang, and B. Tan, *Int. J. Electrochem. Sci.*, 13 (2018) 11388.
31. I. Martinović, G.Z. Zora Pilić, L. Šušić, O. Kowalska, D. Petrović, F. Falak, and J. Mišković, *Int. J. Electrochem. Sci.*, 14 (2019) 4206.
32. W. Zhang, H.-J. Li, M. Wang, L.-J. Wang, Q. Pan, X. Ji, Y. Qin, and Y.-C. Wu, *J. Mol. Liq.*, 293 (2019) 111478.
33. B. Tan, S. Zhang, Y. Qiang, W. Li, H. Li, L. Feng, L. Guo, C. Xu, S. Chen, G. Zhang, *J. Mol. Liq.*, 298 (2020) 111975.
34. S. Tao, and H. Huang, *Int. J. Electrochem.Sci.*, 14 (2019) 5435.
35. P. Singh, D.S. Chauhan, S.S. Chauhan, G. Singh, and M.A. Quraishi, *J. Mol. Liq.*, 286 (2019) 110903.
36. Y. Qiang, S. Zhang, S. Yan, X. Zou, and S. Chen, *Corros. Sci.*, 126 (2017) 295.
37. Z. Shariatinia, and A. Ahmadi-Ashtiani, *J. Mol. Liq.*, 292 (2019) 111409.
38. B. Tan, S. Zhang, Y. Qiang, W. Li, H. Liu, C. Xu, and S. Chen, *J. Mol. Liq.*, 286 (2019) 110891.
39. Y. Qiang, S. Zhang, S. Xu, and W. Li, *J. Colloid Interf. Sci.*, 472 (2016) 52.
40. Y. Qiang, S. Zhang, S. Xu, L. Guo, N. Chen, I.B. Obot, *Inter. J. Electrochem. Sci.*, 11 (2016) 3147.
41. I.B. Obot, Z.M. Gasem, *Corros. Sci.*, 83 (2014) 359.